Analyses of the Northern European summer heatwave of 2018

P. Yiou (1,*), J. Cattiaux (2), D. Faranda (1,3), N. Kadygrov (1), A. Jézéquel (4,6), P. Naveau (1), A. Ribes (2), Y. Robin (2), S. Thao (1), G.J. van Oldenborgh (5), M. Vrac (1)

(1) **Laboratoire des Sciences du Climat et de l'Environnement, UMR8212 CEA-CNRS-UVSQ, IPSL and U Paris Saclay, Gif-sur-Yvette, France.**

(2) **Centre National de Recherches Météorologiques, Université de Toulouse, Météo-France, CNRS, Toulouse, France**

(3) **London Mathematical Laboratory, London, UK**

(4) **Laboratoire de Météorologie Dynamique, UMR CNRS-ENS-UPMC-X, Paris, France**

(5) **KNMI, De Bilt, Netherlands**

(6) **Ecole Nationale des Ponts et Chaussées, Champs-sur-Marne, France**

(*) **Corresponding author:** pascal.yiou@lsce.ipsl.fr

Capsule

A heatwave struck Northern Europe in summer 2018. The probability of this event increased with human-induced climate change. The properties of the atmospheric circulation are not deemed to change.

Introduction

A heatwave struck northern Europe in the summer of 2018. Daily temperature anomalies reached +14K in Scandinavia, the Netherlands and Belgium, which are record-breaking temperatures. This heatwave was exacerbated by a drought caused by a persisting circulation anomaly (Kornhuber et al. 2019; Toreti et al. 2019; World Weather Attribution 2018). The heatwave and drought favored unprecedented forest fires in Scandinavia (NASA Earth Observatory 2018).

This paper aims at characterizing this heatwave event and determining its probability in present and future climate conditions. This paper presents how the 2018 heatwave can be analysed in terms of temperature and atmospheric circulation patterns, and highlights the robustness of the signal to statistical hypotheses.

Defining the event

Defining the spatio-temporal scale of the event is inspired by the procedure of (Cattiaux and Ribes 2018), which consists in selecting the space-time window for which the temperature has been the most extreme (i.e. its probability p is the smallest in present-day conditions). We use E-OBS (Haylock et al. 2008) daily mean temperatures over 1950-2018 and consider each N-day time window between May 1

and October 31, and each n-country connected spatial domain. Overall, we find that the probability p is minimum for the 19-day window between July 15 - August 2 and the 2-country domain covering Finland - Sweden. However this minimum is not sharp and adding Baltic countries, Denmark and Norway to the spatial domain does not significantly change p. Since a larger domain is more robust for the latter analyses, we define the spatial scale as the 5-30°E, 55-70°N area (Fig. 1a). This corresponds to the “Scandinavian cluster” type of heatwave identified by (Stefanon et al. 2012). Over this space-time window, the average temperature anomaly relative to the 1981-2010 climatology is +5.4 K (Fig. 1b), and each single day during this time period in 2018 is more than +3K above the climatological mean seasonal cycle (Suppl. Fig. S1a). The atmospheric circulation is characterized by prolonged high pressure conditions (Fig. 1c) over Scandinavia. This motivates the conditional attribution analysis with respect to the atmospheric circulation, because such circulation patterns generally enhance major heatwaves in the midlatitudes (Quesada et al. 2012; Mueller and Seneviratne 2012), as was observed in summers 2003 (Schaer et al. 2004) or 2010 (Barriopedro et al. 2011).

Unconditional attribution

The unconditional attribution compares the probability p1 of observing the event (exceeding a temperature threshold) in present day or in a climate influenced by human activities (a factual world), and the probability p0 of the event in past conditions or in a climate without human influence (a counterfactual world). We focus on the probability ratio (PR) p1/p0. The results from two different statistical approaches are presented here.

First, we determined p1 and p0 from annual maximum 19-day averaged temperature

over the region in E-OBS data by fitting the period 1950-2017 to a generalized extreme value (GEV) distribution. The location parameter μ is a linear function of a proxy for global warming, for which we take the 4-year smoothed global mean surface temperature (as in (Kew et al. 2019)). This procedure excludes the observed extreme in 2018, as GEV parameter estimates are sensitive to the last value of a time series. The fit was extrapolated to the global temperature of 1900 as a proxy of the pre-industrial climate. The procedure was applied to a few ensembles of transient climate model experiments (EC-Earth2.3 T159 coupled 1860-2018; RACMO 2.2 11km downscaling this EC-Earth ensemble 1950-2018; HadGEM3-A N219 prescribed SST 1960-2015; calibrated Euro-CORDEX ensemble 11km 1971-2018: Fig. 2a). These have realistic variability of 19-day heat extremes: the fitted scale and shape parameters are compatible with the fit to observations. Uncertainty ranges for each dataset were obtained from bootstrapping. Model spread was also added to the model estimates to obtain $\chi^2/dof=1$. We plot the probability ratios and associated uncertainties in Fig. 2a. This diagnostic shows that PR values are significantly larger than 1, with a large range of variations (PR synthesis between models and obervations between 5 and 2000), indicating that such a heatwave is between 5 and 2000 times more likely in the factual simulations.

A second unconditional attribution was performed on the E-OBS dataset and a CMIP5 (Taylor et al. 2012) simulation ensemble using the method of (Ribes et al. 2019). The distribution of mean temperature over the considered space-time domain is assumed to follow a Gaussian distribution, and to covary with a variable representing climate change. This covariate is the summer mean continental temperature over the box -10E-30Ex35N-70N. The probability of the event can be estimated continously in time. This calculation is made for each CMIP5 model and

summarized into a multimodel synthesis. Then, changes in the covariate and the temperature distribution are constrained by E-OBS observations (see Champ DDE for details) Suppl. Fig. S2a. shows the probablity ratio from 1850 to 2100, under the high emission RCP8.5 scenario (Van Vuuren et al. 2011), according to the multimodel synthesis constrained by observations. The effect of human activities on the probability of such event cannot be detected before the end of 20th century as the probability ratio is not significantly different from 1. After the year 2000, the probability ratio is significantly higher than 1 and suggests that human activities have increased the probability ratio of such events. In 2018, the probability of such events has increased by a factor of 39 (95% confidence interval: 3 to 3400, in Suppl. Fig. S2a) due to human activities.

Conditional attribution

We determine the temperature distribution *conditional* to atmospheric patterns that are similar to 2018 changes with time. Following the procedure of (Jézéquel et al. 2018c), we computed analogues of geopotential height at 500mb (Z500) over a zone covering Scandinavia (rectangle in Fig. 1c), which optimizes the temperature/circulation correspondence. The analogues are computed from Z500 in two subperiods (1950-1984; 1985-2018) of the NCEP reanalysis (Kistler et al. 2001). The Z500 data are detrended with a smoothing spline before computing analogues, in order to avoid a bias due to the temperature increase. Ten days (out of 19) yield good analogues (distance < 30^{th} quantile and spatial correlation > 70^{th} quantile). Mean analogue temperatures are simulated by random selections of analogue days from each subperiod, following the procedure of (Jézéquel et al. 2018c). The change of temperature probability distributions describes the thermodynamic changes on a

summer that is similar to 2018. 10000 stochastic samples are generated, with analogues selected in the two subperiods. The changes are significant according to a 2-sided Kolmogorov-Smirnov test (p-value < 10^{-15}).

Although the simulated values do not reach the 2018 record, we find a significant increase of the temperature distribution between the two subperiods (Fig. 2b). This ~1K increase is comparable to the average increase of temperature between the two subperiods. When analogues are selected in RCP8.5 CMIP5 simulations, we find that similar atmospheric patterns lead to summer temperatures that are consistent with the 2018 record values. This means that temperature anomalies of a similar heatwave (same domain, duration, and atmospheric circulation) would reach or exceed 5K by the end of the 21st century (Fig. 2b).

Changes in atmospheric circulation

We diagnosed atmospheric circulation trends by analysing the distance values of the best analogues (Jézéquel et al. 2018a), the local dimension and persistence (Faranda et al. 2017). This was done by comparing the observed Z500 anomaly sequence (in NCEP), and other observed sequences in NCEP or simulated in RCP 4.5 and 8.5 scenarios.

First, we computed the distribution of Z500 distances to the hottest day of the heatwave (17th July 2018) in NCEP and RCP 4.5 and 8.5 scenario simulations. We then counted the number of analogues whose distance is below the 5th quantile of all distances, for each summer. The distance distribution informs on the likelihood to have a similar atmospheric pattern as the observed one (Jézéquel et al. 2018a). We find no significant trend in the number of good analogues in NCEP reanalysis or scenario simulations (Suppl. Fig. S2c): some CMIP5 simulations do identify

marginally significant trends, but there is no consensus among models, as was found for the 2003 heatwave (Jézéquel et al. 2018a).

Second, we computed the *local dimension* of the observed Z500 sequence in CMIP5 RCP4.5 and RCP 8.5 simulations. This assumes that the observed state belongs to the climate variability described by climate models, which is validated by the fact that the distribution of analogue distances for each model is similar to the NCEP reanalysis distances (Rodrigues et al. 2018). The local dimension informs on the number of degrees of freedom of trajectories around a given state and hence on its predictability (Faranda et al. 2017). We find no significant trend in the local dimension of summer 2018 Z500 in CMIP5 RCP4.5 and RCP8.5 simulations.

Third, the *extremal index* informs on the persistence of a given state, i.e. the time it takes to leave its neighborhood in phase space (Faranda et al. 2017). As for the local dimension, the local persistence of summer 2018 Z500 was evaluated on CMIP5 RCP simulations. We find a small but significant decrease of the persistence of these weather patterns (Suppl. Fig. S2d).

Conclusions

This paper refines the preliminary analyses of the World Weather Attribution for that event (World Weather Attribution 2018). Our analyses demonstrate the thermodynamic contribution of human-induced climate change to describe the probability and intensity of the summer 2018 event in Scandinavia. The bulk values and uncertainties of the probability ratios are significantly larger than 1 in two statistical approaches with different underlying technical assumptions. Hence we find a strong and robust contribution of human activities to 2018 heatwave in Northern Europe from the unconditional attribution analysis. This is further supported by an

analysis of record probabilities (see Suppl. Material S2b; (Naveau et al. 2018)). The wide range of probability ratios from the model ensemble calls for a calibration of the model outputs (Bellprat et al. 2019), which is outside the scope of this short paper. Therefore those probability ratios should be used in a qualitative manner, rather than quantitative.

The atmospheric conditions enhance the temperature signal (~+2K, Fig. 2b), but the conditional attribution simulations cannot reach the observed record values, possibly because some physical processes are not taken into account (soil moisture feedbacks and ocean variability).

Those results emphasize the necessity of systematic analyses of European heatwaves (Stefanon et al. 2012), for which the properties of the atmospheric circulation do not change uniformly in scenario simulations (Jézéquel et al. 2018a). This also highlights uncertainties in the changes of atmospheric circulation.

Acknowledgements

This paper was supported by the EUPHEME project, which is part of ERA4CS, an ERA-NET initiated by JPI Climate and co-funded by the European Union (Grant #690462), ERC grant no. 338965-A2C2, and French “Convention de Service Climatique”. The analyses of this paper were obtained with the Climate Explorer (https://climexp.knmi.nl/start.cgi) and the “blackswan” Web Processing Service (https://github.com/bird-house/blackswan).

References

Barriopedro, D., E. M. Fischer, J. Luterbacher, R. M. Trigo, and R. García-Herrera,

2011: The hot summer of 2010: redrawing the temperature record map of Europe. *Science*, **332**, 220–224.

Bellprat, O., V. Guemas, F. Doblas-Reyes, and M. G. Donat, 2019: Towards reliable extreme weather and climate event attribution. *Nature communications*, **10**, 1732.

Cattiaux, J., and A. Ribes, 2018: Defining single extreme weather events in a climate perspective. *Bulletin of the American Meteorological Society*, https://doi.org/10.1175/BAMS-D-17-0281.1.

Faranda, D., G. Messori, and P. Yiou, 2017: Dynamical proxies of North Atlantic predictability and extremes. *Scientific reports*, **7**, 41278.

Haylock, M. R., N. Hofstra, A. M. G. K. Tank, E. J. Klok, P. D. Jones, and M. New, 2008: A European daily high-resolution gridded data set of surface temperature and precipitation for 1950-2006. *J. Geophys. Res. - Atmospheres*, **113**, doi:10.1029/2008JD010201.

Jézéquel, A., J. Cattiaux, P. Naveau, S. Radanovics, A. Ribes, R. Vautard, M. Vrac, and P. Yiou, 2018a: Trends of atmospheric circulation during singular hot days in Europe. *Environmental Research Letters*, **13**, 054007.

——, P. Yiou, and S. Radanovics, 2018b: Role of circulation in European heatwaves using flow analogues. *Climate Dynamics*, **50**, 1145–1159.

Kew, S. f, S. Y. Philip, G. Jan van Oldenborgh, G. van der Schrier, F. E. Otto, and R. Vautard, 2019: The Exceptional Summer Heat Wave in Southern Europe 2017. *Bulletin of the American Meteorological Society*, **100**, S49–S53.

Kistler, R., and Coauthors, 2001: The NCEP-NCAR 50-year reanalysis: Monthly means CD-ROM and documentation. *Bulletin of the American Meteorological Society*, **82**, 247–267.

Kornhuber, K., S. Osprey, D. Coumou, S. Petri, V. Petoukhov, S. Rahmstorf, and L. Gray, 2019: Extreme weather events in early summer 2018 connected by a recurrent hemispheric wave-7 pattern. *Environmental Research Letters*, **14**, 054002.

Mueller, B., and S. I. Seneviratne, 2012: Hot days induced by precipitation deficits at the global scale. *Proc. Natl. Acad. Sci. USA*, doi:10.1073/pnas.1204330109, https://doi.org/10.1073/pnas.1204330109.

NASA Earth Observatory, 2018: Scarcely Seen Scandinavian Fires. https://earthobservatory.nasa.gov/images/92454/scarcely-seen-scandinavian-fires (Accessed September 6, 2019).

Naveau, P., A. Ribes, F. Zwiers, A. Hannart, A. Tuel, and P. Yiou, 2018: Revising return periods for record events in a climate event attribution context. *Journal of Climate*, **31**, 3411–3422.

Quesada, B., R. Vautard, P. Yiou, M. Hirschi, and S. I. Seneviratne, 2012: Asymmetric European summer heat predictability from wet and dry southern winters and springs. *Nature Climate Change*, **2**, 736–741, https://doi.org/Doi 10.1038/Nclimate1536.

Ribes, A., S. Thao, and J. Cattiaux, submitted: Describing the relationship between a weather event and climate change: a new statistical approach. *submitted to J. Clim.*, https://hal.archives-ouvertes.fr/hal-02122780/document.

Rodrigues, D., M. C. Alvarez-Castro, G. Messori, P. Yiou, Y. Robin, and D. Faranda, 2018: Dynamical properties of the North Atlantic atmospheric circulation in the past 150 years in CMIP5 models and the 20CRv2c Reanalysis. *Journal of Climate*,.

Schaer, C., P. Vidale, D. Luthi, C. Frei, C. Haberli, M. Liniger, and C. Appenzeller, 2004: The role of increasing temperature variability in European summer heatwaves. *Nature*, **427**, 332–336.

Stefanon, M., F. D'Andrea, and P. Drobinski, 2012: Heatwave classification over Europe and the Mediterranean region. *Environmental Research Letters*, **7**, 014023.

Taylor, K. E., R. J. Stouffer, and G. A. Meehl, 2012: An Overview of CMIP5 and the Experiment Design. *Bull. Amer. Met. Soc.*, **93**, 485–498.

Toreti, A., and Coauthors, 2019: The exceptional 2018 European water seesaw calls for action on adaptation. *Earth's Future*, **7**, 652–663.

Van Vuuren, D. P., and Coauthors, 2011: The representative concentration pathways: an overview. *Climatic change*, **109**, 5.

World Weather Attribution, 2018: Heatwave in northern Europe, summer 2018. https://www.worldweatherattribution.org/attribution-of-the-2018-heat-in-northern-europe/ (Accessed September 6, 2019).

Figures

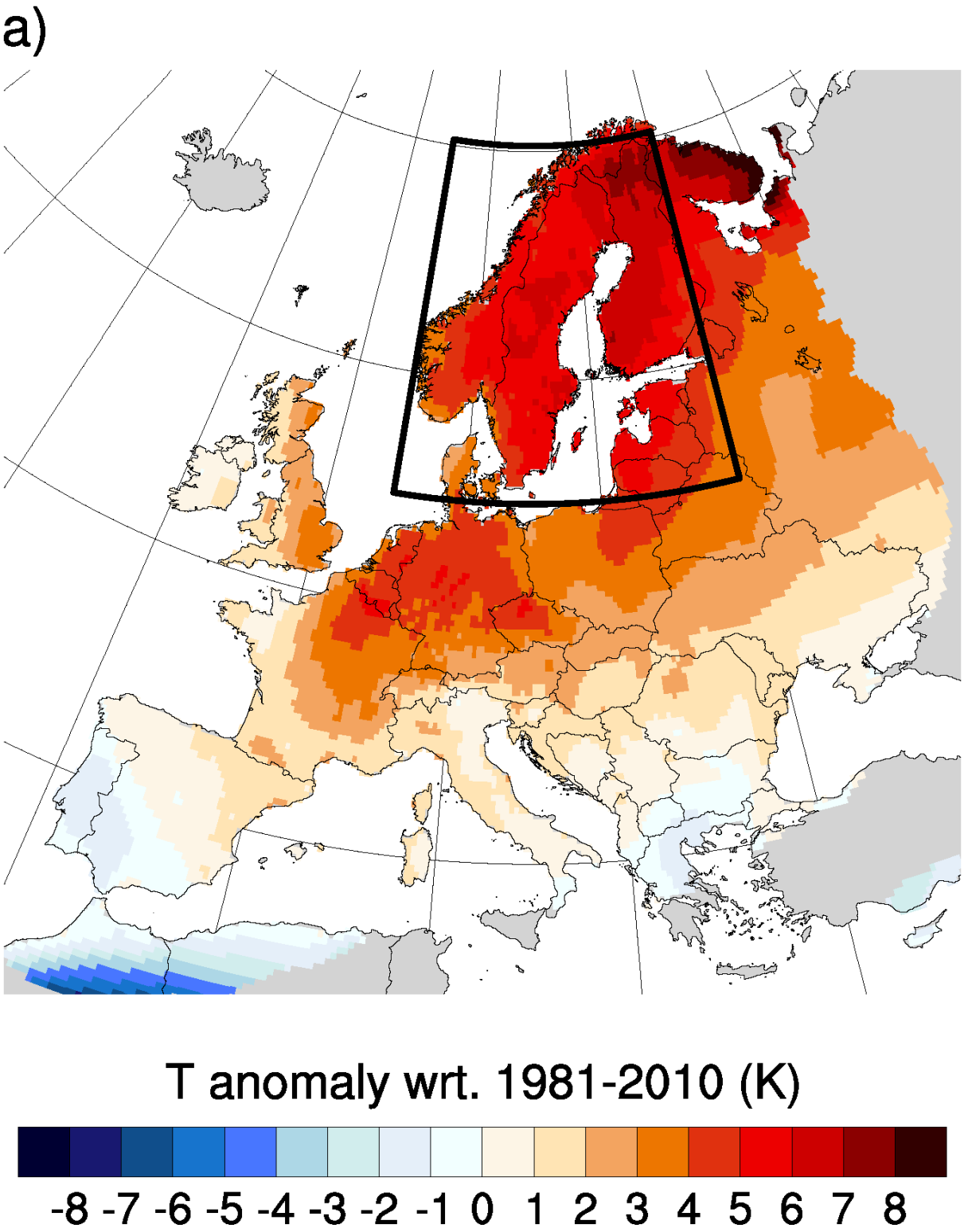

Panel 1a

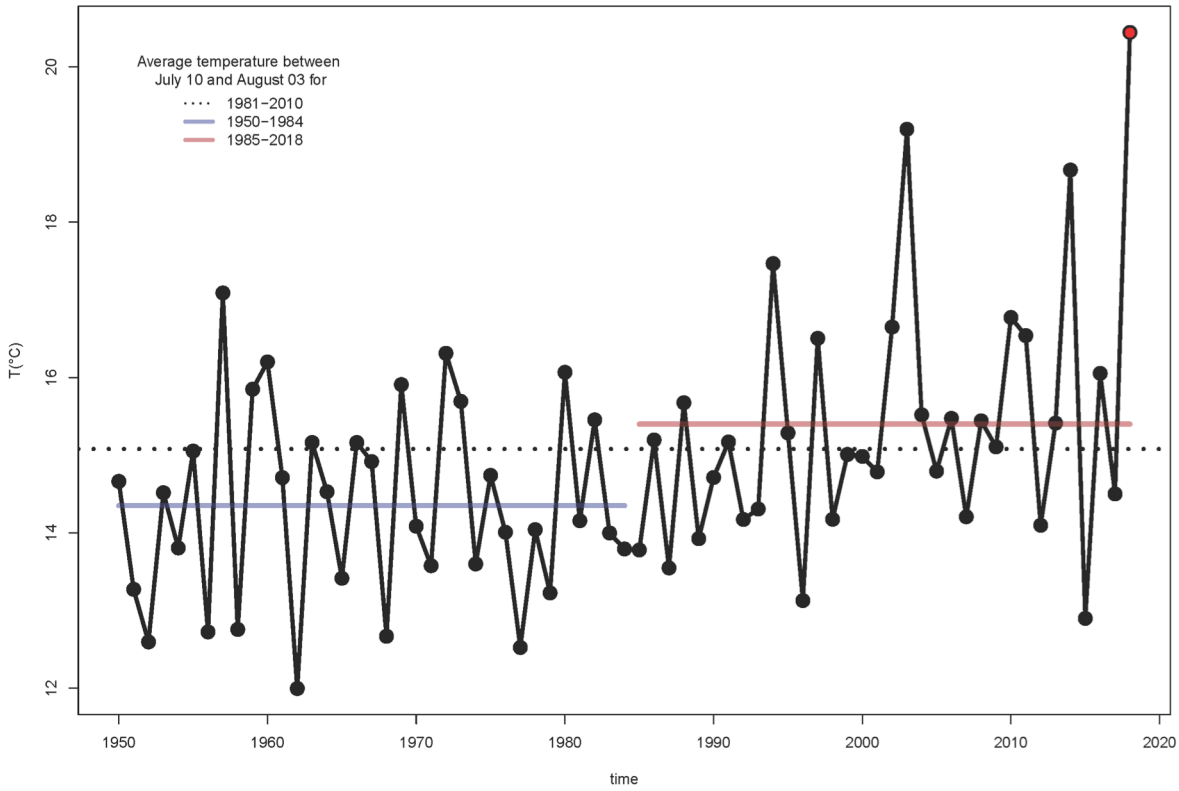
Average temperature between
July 10 and August 03 for
1981−2010
1950−1984
1985−2018
T(°C)
12
14
16
18
20
1950
1960
1970
1980
1990
2000
2010
2020
time

4 **Panel 1b**

5

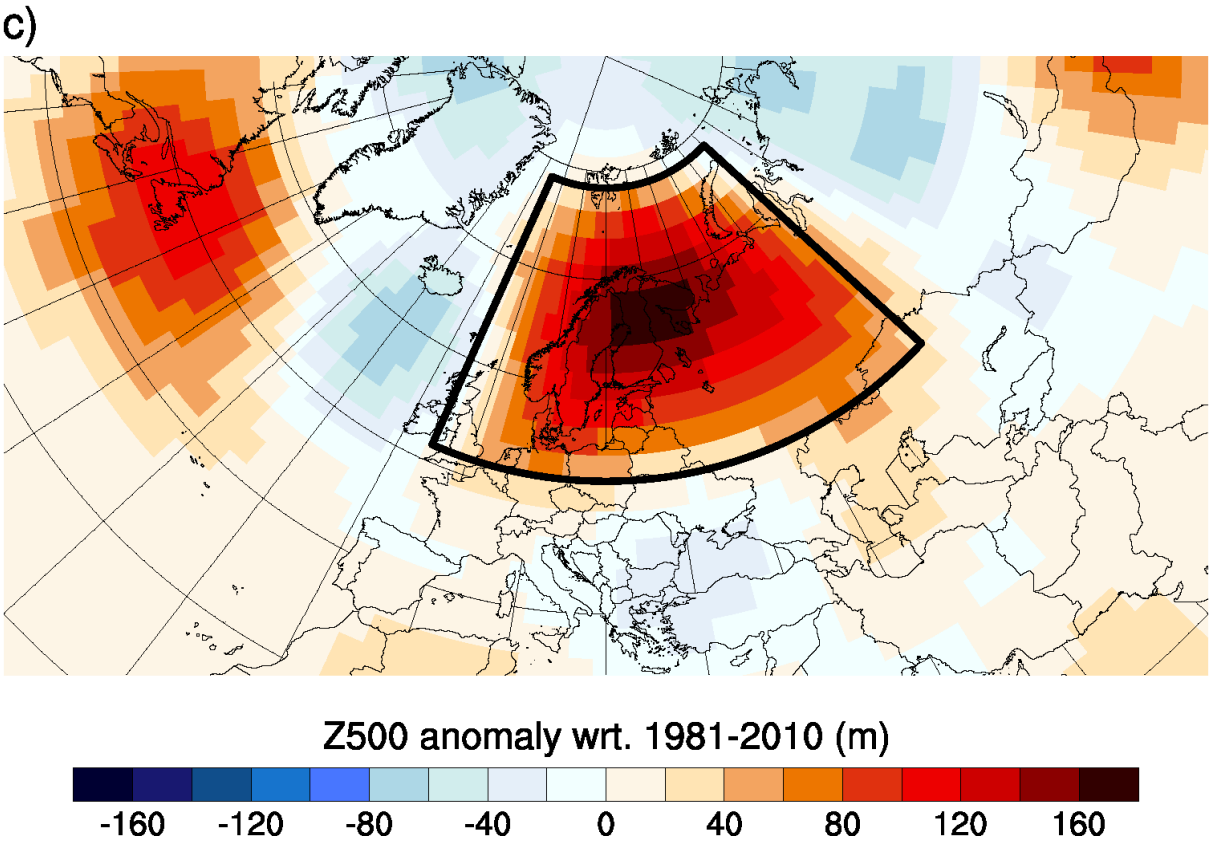

Panel 1c

Figure 1: Geographical and temporal features of the event from reanalyses & observations. **Panel a**. Map of Temperature Anomalies in E-OBS between July 15th 2018 and August 2nd 2018, with respect to a 1981-2010 climatology. The rectangle indicates the zone to be analyzed (e.g. Scandinavia). **Panel b.** Time series of spatial (rectangle in a) & temporal (15 July to 2 August) average temperature (E-OBS) from 1950 to 2018, with reference 1981-2010 climatology. **Panel c.** Anomalies of Z500 in NCEP over the North Atlantic between July 15th 2018 and August 2nd 2018, with respect to the 1981-2010 climatology. The rectangle indicates the zone for the computation of analogues.

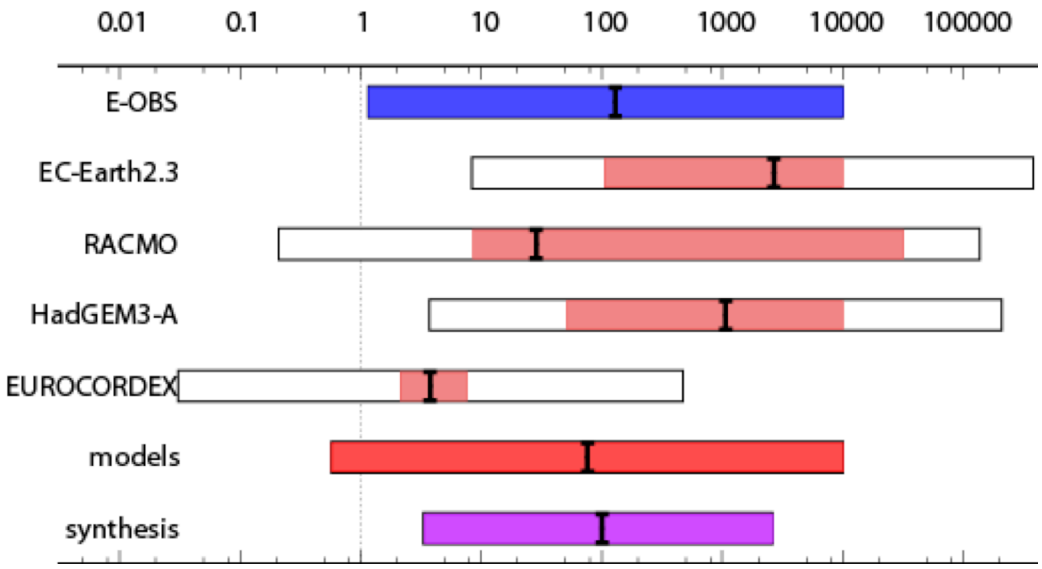

Panel 2a

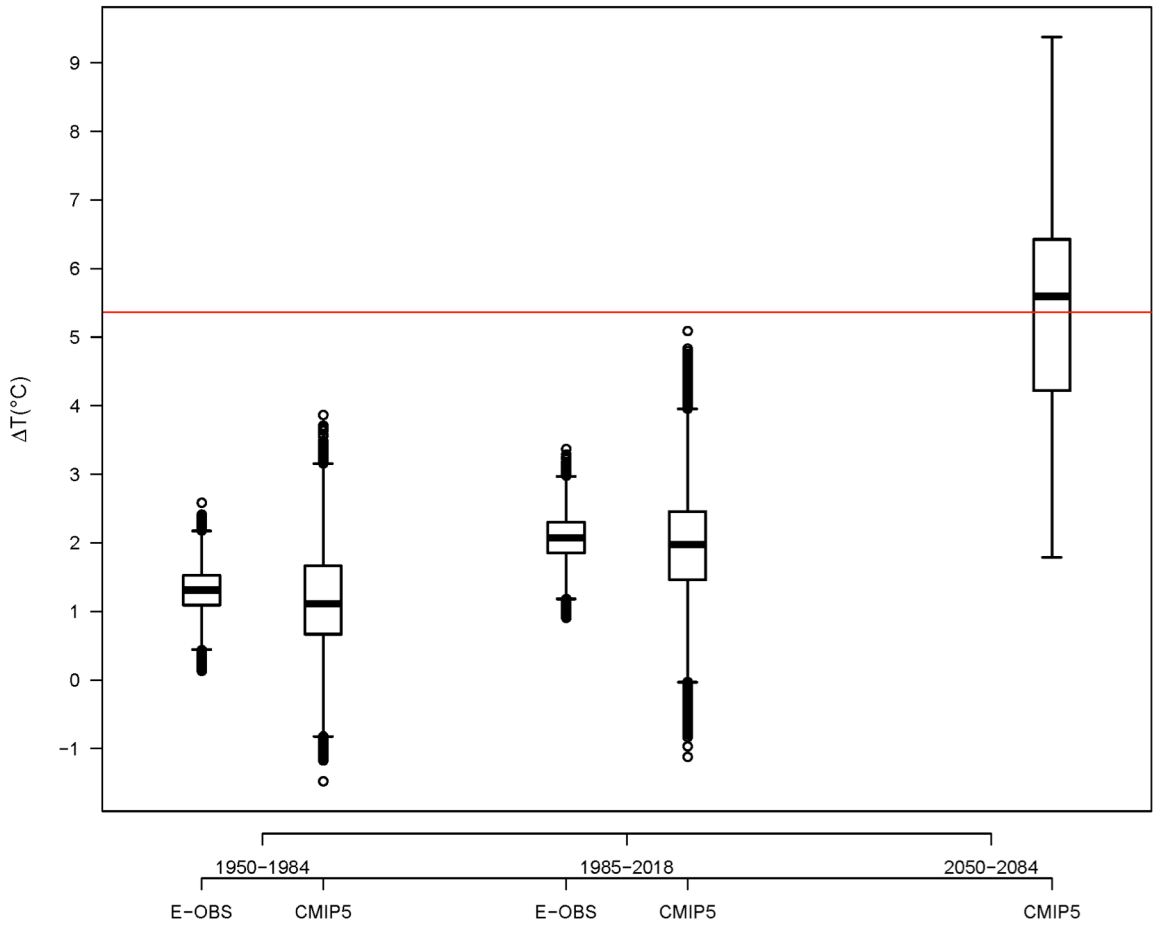

Panel 2b

Figure 2. Panel a. Probability ratios (PR) from observations (E-OBS) in blue, and climate model simulations (EC-EARTH, RACMO, HadGEM3, Euro-CORDEX ensemble) in pink, all models in red, and observation-model synthesis in purple. The black vertical lines indicate the value of the best fit. The white boxes represent the model spread that is added to the pink boxes representing a conservative uncertainty due to natural variability to obtain $\chi^2/dof=1$. **Panel b**. Conditional temperature simulations in CMIP5 and in E-OBS for different periods. The boxplots represent the temperature distributions, conditioned to the atmospheric circulation observed during event that are simulated through the analogue procedure for different periods. For the CMIP5 models, the temperatures are simulated independently for each model and the boxplots represent the distribution of all the temperatures simulated for the CMIP5 models altogether. The circle points on the boxplots represent the simulated temperatures that are 1.5 times the interquartile range above the upper quartile and bellow the lower quartile. The red line denotes the value of the observed mean temperature between July 15 and August 2 2018.